The Saffman–Taylor instability: From the linear to the circular geometry

H. Thomé, M. Rabaud, V. Hakim, and Y. Couder
Groupe de Physique des Solides de l'Ecole Normale Supérieure, 24 rue Lhomond, 75231 Paris Cedex 05, France

(Received 3 May 1988; accepted 25 October 1988)

The Saffman–Taylor fingers are studied in cells that have the form of sectors of a disk. The less viscous fluid can be injected at the apex (divergent flow) or at the periphery (convergent flow). As in the linear geometry, at large velocities, a unique finger tends to occupy a well determined fraction λ of the cell angular width. This fraction is a function of the angle of the cell, being larger than 0.5 in the divergent case and smaller in the convergent case. In both cases these fractions tend linearly toward $\lambda = 0.5$ when the angle of the cell tends to zero. In support of recent theories, these results show how the selection is changed when the geometry induces an increase or a decrease of the curvature of the profiles. The formation of fingers in the circular geometry is revisited. In a divergent flow, the circular front appears to break into independent parts so that each finger grows as if it were contained in a sector shaped cell. The rate of occupancy of the cell by one of the fluids as a function of the distance to the center is then discussed. Finally, the existence of the mathematical counterpart to the well-known Saffman–Taylor finger solutions in a nonparallel cell is discussed in the Appendix.

I. INTRODUCTION

The nonlinear growth of Saffman–Taylor fingers at large amplitude has been investigated in two geometries until now. The cell initially used by Saffman and Taylor[1] was a long narrow Hele–Shaw channel with parallel walls. The axisymmetric geometry was introduced by Bataille[2] and further investigated by Paterson.[3] It is a circular cell where the less viscous fluid can be injected either at the center, creating a divergent flow, or at the periphery, creating a convergent flow. These two geometries, linear and circular, appear at first sight very different and have given rise to different types of analysis.

In the circular case the experimental situation is basically unsteady because the perimeter of the front either increases (divergent flow) or decreases (convergent flow) as the pattern grows. In the divergent case, which has been more widely investigated, the first destabilization creates several fingers that grow simultaneously. As they reach a larger perimeter, they in turn destabilize by tip splitting so that complex patterns are formed. Attempts at interpretation of the finger shapes are due to Paterson,[3] Howison,[4] and Bensimon and Pelcé.[5] The statistical properties of these patterns have been investigated by Rauseo *et al.*,[6] Ben Jacob *et al.*,[7] and Sander,[8] and compared by these authors to fractal structures.

In the channel with parallel walls, on the other hand, it is possible to reach nearly stationary experimental conditions where a steady solution of the finger shape is reached. This situation is attractive and much effort has been devoted to the understanding of the selection of the physically observed fingers. Reviews on this problem can be found in Saffman,[9] Bensimon *et al.*,[10] and Homsy.[11] These reviews are, however, anterior to some recent findings quoted below. Here we must summarize the main results.

Saffman and Taylor[1] showed that in the parallel channel there exists (if surface tension is neglected) an analytical expression for the possible fingers shapes. The axis Ox being taken along the cell's length in the middle of its width, the two lateral walls are at $y = \pm W/2$. The solutions are then

$$x = s[W(1-\lambda)/\pi]\log\cos(\pi y/\lambda W)\,, \tag{1}$$

where λ, the parameter of the family of profiles, is the ratio of the width occupied by the less viscous fluid over the width of the cell. (The parameter s is $+1$ for fingers traveling in the direction of increasing x and -1 for fingers traveling in the opposite direction.) These solutions are both solutions of Laplace equation $\nabla^2 p = 0$ (where p is the pressure inside the viscous fluid) at a given time, and dynamically steady solutions of the problem which, as they move, simply translate along the channel.

At large velocities, the physically observed fingers are selected among solutions of Eq. (1). Two types of selection processes have been observed.

(i) *Normal fingers:* In the classical case, first described by Saffman and Taylor,[1] the finger at large velocities tends to occupy half of the channel. It is only recently that the selection mechanism of this finger was fully understood. Following a numerical study by Vanden-Broeck,[12] researchers such as Combescot *et al.*,[13] Shraiman,[14] and Hong and Langer[15] have shown analytically how capillary forces select the observed solution. Surface tension acting on the profile creates corrective terms that can be calculated by the Wentzel–Kramers–Brillouin method. These terms create a singular situation at the tip; in order to maintain a continuous derivative along the profile it is necessary to satisfy a solvability condition. As a result, only a discrete set of solutions is selected. They all have a relative width λ larger than 0.5, which tends toward this value when capillary effects vanish.

(ii) *Anomalous fingers:* We showed experimentally in previous works (Couder *et al.*[16] and Rabaud *et al.*[17]) that a completely different type of selection is obtained when a local disturbance affects the tip of the finger (for instance a groove etched in the glass plates along the axis of the cell). The resulting fingers still have the shapes of members of the

 0899-8213/89/020224-17$01.90

family of solutions given by Eq. (1), but they are selected by their radius of curvature ρ at their tip. As a result, fingers with widths smaller than one-half can then be observed. In a large range of velocities V, ρ is proportional to $V^{-1/2}$. This selection makes these fingers close analogs of the crystalline dendrites. They also resemble dendrites in their general shape and their stability. Their extremity is stabilized by the perturbation so that the finger only destabilizes by the growth, along its sides, of a wave giving rise to lateral side branches. At very large velocities, a saturation is observed when ρ becomes of the order of magnitude of the cell's thickness (it then remains constant at $\rho \approx 2.2b$). These anomalous fingers have since been observed by Zocchi *et al.*[18] and Kopf-Sill and Homsy[19] and discussed theoretically by Hong and Langer.[20]

The basic idea of the present work is to observe both these selective processes in action in a different geometry with other boundary conditions. We first undertook disturbing slightly the conditions of the linear cell by having a gradually varying width. Depending on whether the finger travels in the direction of increasing or decreasing width, the curvature along its profile (for a given λ) is increased or decreased. As a result we expected a change in the selected solutions. We will see that we were able to extend this investigation to the cases where the walls diverge at a large angle. The results can then be used to interpret the nonlinear behavior of the fingers in the circular geometry.

The remainder of this paper will be divided into three sections. In the first section (Sec. II) we will describe the experimental setup; in the second section (Sec. III) we will report the results concerning sector shaped cells and discuss the finger shapes, their selection, and their stability. In the third section (Sec. IV) we will recall some of the characteristics of the patterns obtained in the circular cells and show how we can interpret them using the results obtained in sector shaped cells. Finally, in the Appendix, we present partial results about the mathematical self-similar counterpart of the well-known continuum family of solutions obtained by Saffman and Taylor.[1]

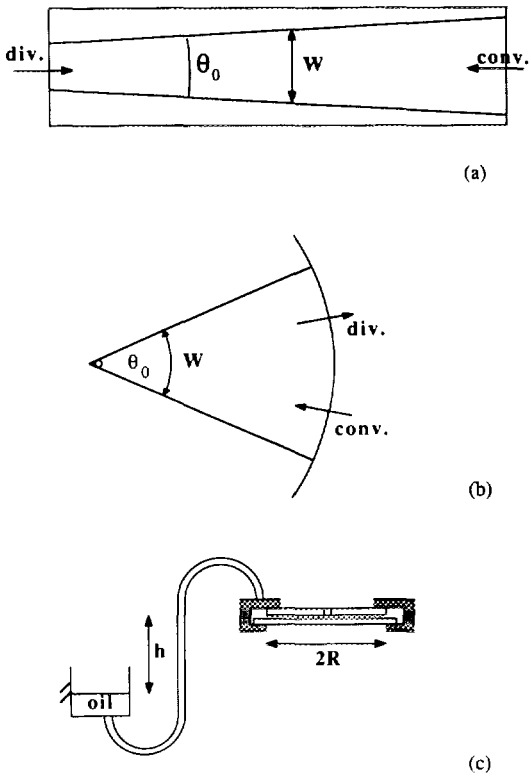

FIG. 1. Here we see a (a) sketch of the small angle cell, (b) sketch of the large angle cell, and (c) section of the circular cell showing the injection system.

II. EXPERIMENTAL SETUP

A. Cells

We built a new cell for each value of the angle we wished to investigate. For small values of this angle ($\theta_0 \approx \pm 6°$), the channel was built as a linear cell but with tapered lateral sides [Fig. 1(a)]. The plates were made of float glass 1.5 cm thick. They were 150 cm long and 32 cm wide. The plate spacing was (as in all the other cells) $b = 0.1$ cm. For larger values of the angle (15° and 30°) the lateral walls actually met. At their meeting point a hole was drilled through the top glass plate. In this way air could be injected (in the divergent case) or oil pumped out (in the convergent case) at the apex of the angle. (The glass plates being longer, the channel was completed with a wide linear section.) Finally, for very large angles (40°–180°) a sector of a circular cell of diameter 50 cm was used. Radial spacers were placed at the desired angle and the plates were clamped over them [Fig. 1(b)].

In order to obtain anomalous fingers we could stretch a thin nylon wire (100 μm in diameter) along the axis of the cell.

The most viscous fluid was either a silicon oil Rhodorsyl 47 V 100 with viscosity $\mu = 96.5 \times 10^{-3}$ kg/m sec at 25 °C and surface tension $T = 20.9 \times 10^{-3}$ N/m, or a silicon oil 47 V 20 with $\mu = 19 \times 10^{-3}$ kg/m sec at 25 °C and $T = 20.7 \times 10^{-3}$ N/m. The less viscous fluid was air or nitrogen.

B. Injection

The flow in a given direction could be forced in two ways. We could inject air at one end of the cell from a high pressure gas cylinder through a series of pressure reducing valves. A flow meter showed that in this case a nearly constant volumic rate of injection was obtained. In the circular cell we could also extract oil from the periphery. For this purpose the periphery of the cell formed a toroidal airtight reservoir [a section of it is shown in Fig. 1(c)]. This reservoir was connected to a larger vessel opened at the top. The cell, the reservoir, and part of the vessel were first filled with oil. The vessel was then lowered so that oil was siphoned out of the cell by hydrostatic pressure and air penetrated at the center. The level of the free surface in the vessel was maintained constant by an overflow pipe that evacuated the withdrawn oil [Fig. 1(c)]. This technique provided a constant applied pressure measured by a pressure gauge.

Both techniques were used because they resulted in dif-

ferent velocity evolution along the cell and also created different flexions of the glass plates.

With the constant rate of injection the velocity of the finger can, in a first approximation, be deduced from the geometry. Insofar as the finger retains the same type of shape (self-similar growth), the width of a divergent finger increases linearly with the distance r_0 from the apex it has reached. Its velocity then decreases as $1/r_0$. A convergent finger for the same reason will become narrower and its velocity will increase as $1/r_0$.

With constant pressure pumping, the local velocity has to be deduced from the Darcy law:

$$\mathbf{V} = -(b^2/12\mu)\nabla p . \tag{2}$$

It is nontrivially related to the distance r_0 from the center. A divergent finger will slow down at the beginning of its growth, because the curvature of the isobar decreases with r_0. When it approaches the extremity of the cell, it will accelerate because the difference of pressure between the two extremities is applied on a decreasing length. In the same experimental conditions a convergent finger will have, near the apex, a steadily increasing velocity because both effects will now be of the same sign. A complete derivation of the velocity of a circular front is given in Sec. IV A 1.

C. Flexions of the plates

In the classical cells with parallel walls, the glass plates are clamped together on their lateral sides at a distance W, and for narrow cells the flexions can usually be neglected. Flexions become a matter of concern in the sector shaped cells and are the main limiting factor in experiments in circular cells.

An estimate of the effect in this later case can be obtained. We will only consider a circular cell in which a constant excess of pressure δp has been applied. The increase of the plate spacing δb is maximum at the center and can be calculated from the flexions of the two glass plates of radius R and thickness e (with clamped boundaries, $b = b_0$ and $\partial b/\partial r = 0$ in $r = R$);

$$\delta b = 2\{[3(1-\sigma^2)/16E](\delta p R^4/e^3)\}, \tag{3}$$

where E is the Young modulus of the glass and σ the Poisson coefficient.

In fact, the experimental situation is more complicated because a gradient of pressure exists in the cell so that (3) gives only an upper limit of the effect. Furthermore, the distribution of pressure changes with time. In the case where injection of air at the center is used, the deformation of the plates increases during the pattern's growth and the plates spacing tend to widen in front of the growing fingers. This dynamical increase of b tends to accelerate the front.

When oil is extracted out of the periphery, the flexions are of opposite sign and maximum at the beginning of the experiment. Flexions decrease as air at atmospheric pressure penetrates the cell so that, again, the advancing fingers move in a region where b tends to increase with time. However, the directions of the thickness gradient are opposite in the two cases.

In the experiments presented here we have limited δp to 1% of the atmospheric pressure. We have measured the deformation of the plates and checked that we always had $\delta b/b \leqslant 0.02$.

D. Visualization

The velocity of the fingers and their width were measured using videotape recordings and hard copies of the screen images. The finger shapes were analyzed on photographs that showed the profile with more precision.

III. THE SECTOR OF A DISK GEOMETRY: RESULTS AND INTERPRETATION

A. Normal fingers

With nonparallel cells, we lose the translational invariance and the possible stationarity of the solutions.

Experimentally, the actual control parameter is either the pressure or the flow rate, and the velocity of the front results from the value of this parameter. In tapered cells, as the finger grows, the width of the channel varies and the velocity becomes time dependent. The value of the angle θ_0 is a measure of the unsteadiness imposed by the geometry during the growth. Small angles will correspond to a quasistatic limit and we will present this case first.

1. Small angles ($\theta_0 = 0°$ and 6°)

We first performed a series of experiments intended to compare the fingers' shape and selection in a traditional parallel cell of constant width $W = 12$ cm, and in a cell with gradually varying width.

In the parallel case the experimental evolution of the width λ with increasing velocity is in perfect agreement with previous results, when expressed in terms of the dimensionless number $1/B$:

$$\frac{1}{B} = \frac{12\mu V}{T}\left(\frac{W}{b}\right)^2, \tag{4}$$

where W and b are the width and the thickness of the cell, respectively, μ the viscosity of the most viscous fluid, T the surface tension, and V the velocity of the finger. This dimensionless number was introduced by Tryggvason and Aref[21] and used by Park and Homsy[22] and Tabeling *et al.*,[23] who showed that the data about the finger selection obtained in all linear cells were almost reconciled by its use. To understand why $1/B$ is the relevant parameter we can note that it can be written

$$\frac{1}{B} = 12\pi^2\frac{W^2}{l_c^2} \approx 118.4\frac{W^2}{l_c^2}, \tag{5}$$

where l_c is the wavelength of maximum instability of a plane interface moving at velocity V, given by the linear stability analysis of Chuoke *et al.*[24]:

$$l_c = 2\pi/k_c = \pi b\sqrt{T/\mu V} . \tag{6}$$

Therefore $1/B$ measures how far the geometrical length scale W is from the length scale of spontaneous destabilization.

The cell with slightly tapered lateral walls was designed so that the angle between the two sides was $\theta_0 = 6°$. The apex

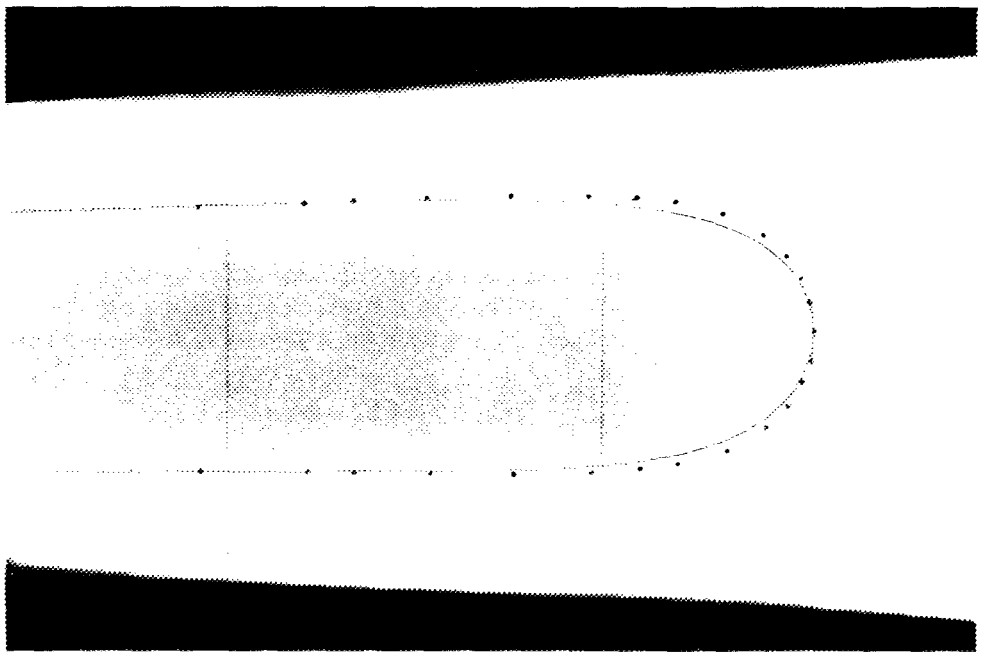

(a)

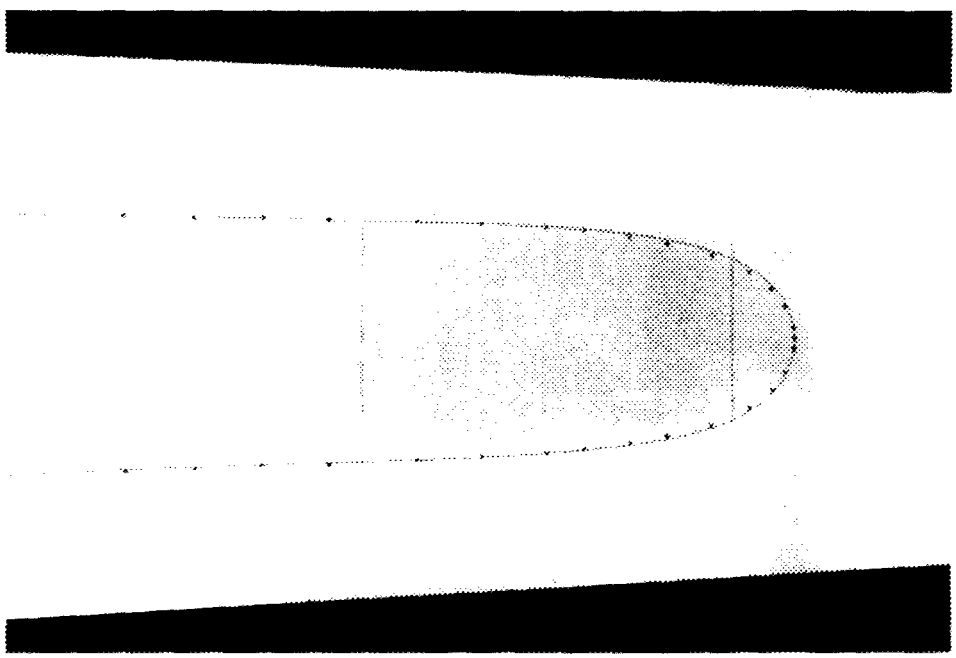

(b)

FIG. 2. Fingers obtained at large velocities: (a) in a cell with $\theta_0 = 6°$, the finger moving in the divergent direction, $\lambda = 0.54$; and (b) in a cell with $\theta_0 = -6°$, the finger moving in the convergent direction, $\lambda = 0.46$. The dots show the best fits with the approximate solutions given by Eq. (8).

of the angle was far out of the cell and the width of the cell at midlength was also 12 cm. Figures 2(a) and 2(b) show the shape of fingers moving in this cell, respectively, in the widening and narrowing directions. In order to describe the finger width, we will consider the same region of the cell where the width is 12 cm, and vary the velocity to reach different values of $1/B$ in this region. If we measure the width of the finger far from its tip in this region of the channel, we observe a dependence on $1/B$ that is very similar to that observed in the linear case. However, the limit values of λ at large velocities are different from the value $\lambda = 0.48$ obtained in channels with parallel sides. (Here 0.48 differs from the ideal value 0.5, as shown by Tabeling *et al.*[23]) We find $\lambda_0 = 0.50 \pm 0.01$ when the finger moves in the direction of the widening channel (divergent finger), and $\lambda_0 = 0.46 \pm 0.01$ when it moves in the narrowing direction (convergent finger).

An approximate solution for the finger shape in the ab-

sence of surface tension can be obtained by transforming the solution given by Eq. (1). Our geometry is in the shape of a sector of a disk. We choose the apex of the angle as the origin and call θ_0 the value of the angle. The axis Ox is the bisector of this angle. By a series of successive conformal transformations it is easy to show that if we write

$$r = r_0 \exp(\theta_0 x/W) \quad \text{and} \quad \theta = \theta_0 y/W, \tag{7}$$

we transform the boundaries of the parallel cell into those of a sector shape with an angle θ_0. (We have simultaneously gone from Cartesian coordinates to polar ones.) Because of the potential nature of the flow, the transformed of the isobars in the first geometry will be isobars in the second one. By applying transformation (7) to the solutions given by (1), we find

$$r = r_0[\cos(\pi\theta/\lambda\theta_0)]^{s(1-\lambda)(\theta_0/\pi)}, \tag{8}$$

with $-\theta_0/2 < \theta < \theta_0/2$ and $\theta_0 < 2\pi$.

In order to compare Eq. (8) to the real fingers, we have used r_0, the distance of the fingertip to the origin, as the scaling factor. The finger profiles obtained with $s = +1$ correspond to fingers moving in the divergent direction $s = -1$ to convergent fingers. The convergent profiles when $r \to \infty$ and the divergent profiles when $r \to 0$ tend toward asymptotes given by $\theta_{\max} = \pm\lambda\theta_0/2$.

We must emphasize that these are not exact solutions of the problem. By using the conformal mapping we have transformed a solution, at a given time, of the Laplace equation in the linear channel into a solution at a given time in a sector shaped cell. But the solutions given by Eq. (1) were also dynamical solutions and these fingers had translational invariance along the cell. *This invariance is not transformed into self-similarity by the conformal transformation* (such a transformation does not preserve the gradients). In other terms a finger with a shape given by Eq. (8) can exist at a given time, but it will not grow into a similar finger at a later time (for more details see the Appendix).

However, for small values of θ_0, the observed fingers in the asymptotic regime are very close in shape to the solutions of Eq. (8), as is shown in Fig. 2. For this reason, and as long as θ_0 is small, we can consider the solutions given by (8) as approached solutions. A few interesting characteristics can be noticed. We calculate the curvature K at the tip where $\theta = 0$;

$$K(\theta = 0) = -\frac{1}{r_0}\left[s\left(\frac{1-\lambda}{\lambda^2}\right)\frac{\pi}{\theta_0} + 1\right]. \tag{9}$$

In order to compare it to the curvature of the finger in a linear geometry, we can note that the local width of the cell at r_0 is $W = \theta_0 r_0$. Expressed in terms of W, the curvature becomes

$$K(\theta = 0) = -s\frac{\pi}{W}\left(\frac{1-\lambda}{\lambda^2}\right) - \frac{\theta_0}{W}. \tag{10}$$

The first term is the curvature of the finger in a linear cell of width W, the second is the curvature added by the geometry. In the divergent case both contributions are of the same sign, so that for given λ and W, the curvature is larger than in a parallel cell. In the convergent case the terms are of opposite sign and the curvature smaller. However, in the experiment, the divergent fingers actually observed at large velocity [Fig. 2(b)] have a smaller curvature at the tip than the convergent ones [Figs. 2(a) and 2(b)], because the selected values of λ in the former case are larger than in the latter one.

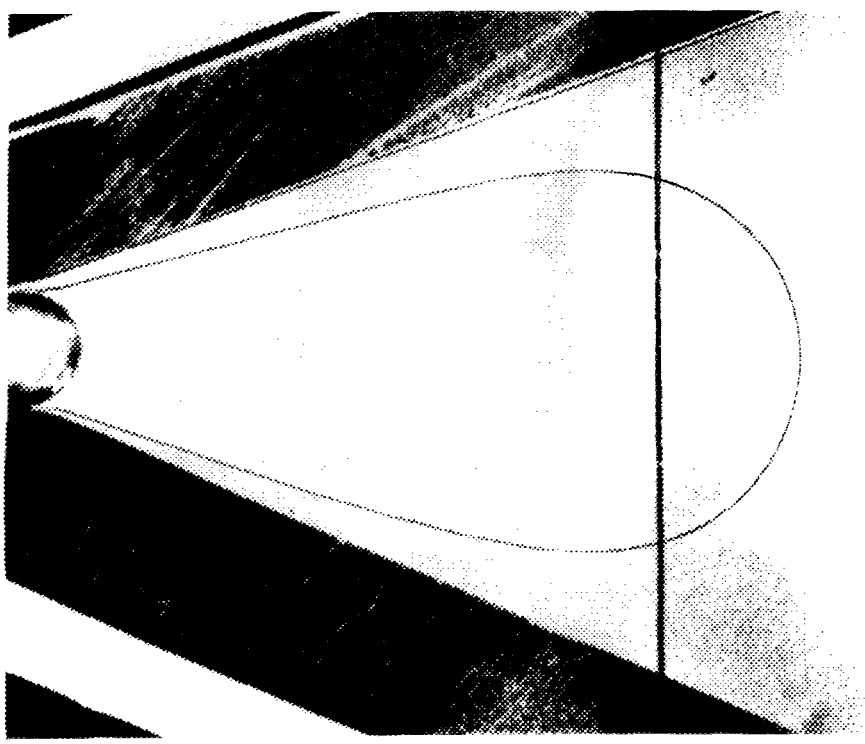

FIG. 3. At low velocity in a divergent cell, $\theta_0 = 43°$, the finger has a constantly decreasing relative width.

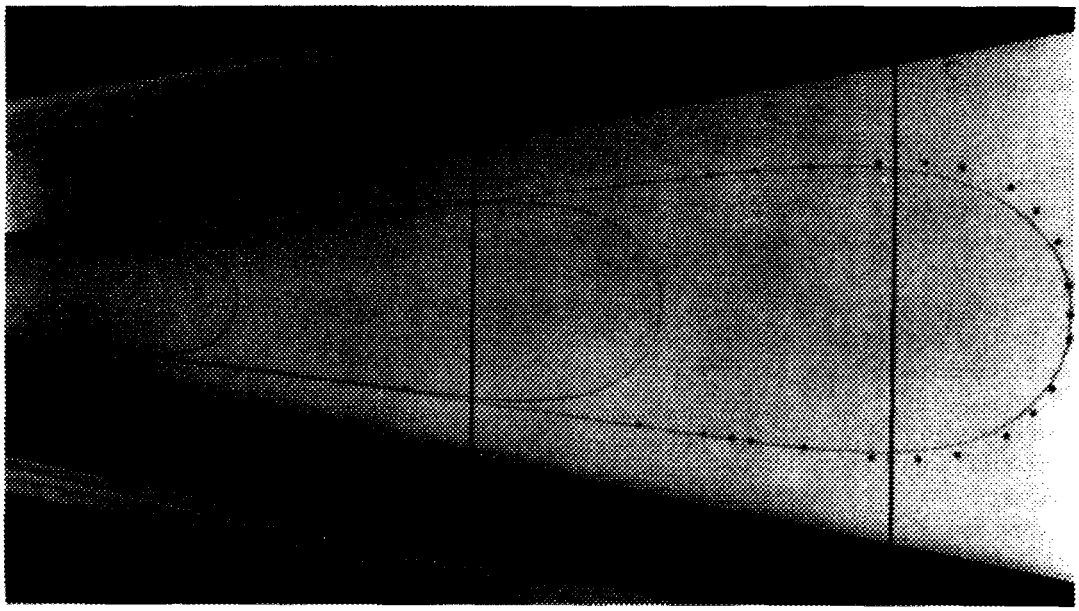

(a)

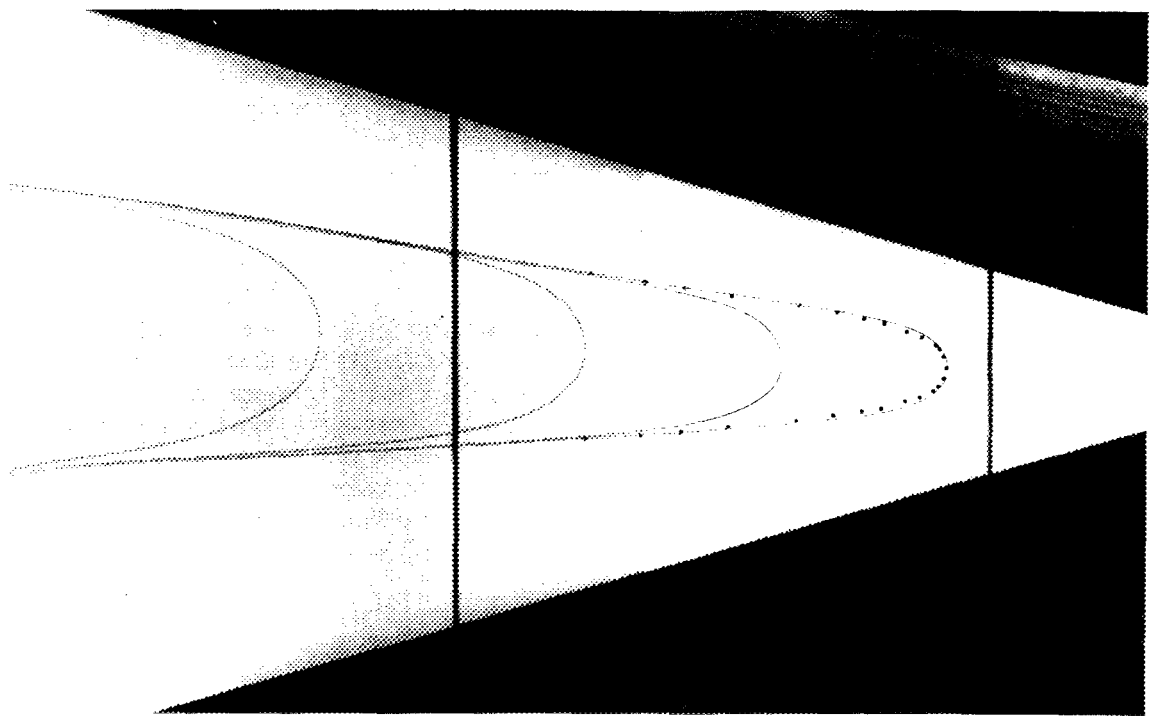

(b)

FIG. 4. Superimposition of successive photographs showing that at large velocities the fingers have self-similar shapes as they grow. (a) Divergent case, $\theta_0 = 23°$, $\lambda = 0.64$, (b) convergent case, $\theta_0 = -32°$, $\lambda = 0.38$. Dots are the best fit by Eq. (8).

2. Large angles ($\theta_0 > 10°$)

The cell is now in the shape of a sector of a disk and the air is injected either at the apex or at the periphery. In the divergent case there is direct formation of one single finger (whenever $\theta_0 < 90°$) that moves outward.

In the convergent case the air penetrates at the periphery forming several fingers at the scale of l_c [Eq. (6)]. These fingers compete and screen each other off. Finally only one finger survives and moves at increasing speed toward the origin of the cell. These fingers are very stable, they are narrow, and not necessarily well centered in the middle of the cell. It is worth noting that this process is not limited to small

angle cells and is observed in cells of all angular widths up to $\theta_0 = 360°$.

a. Finger shapes. As seen previously, in each region of the cell, the finger width reaches a limit value, which will be characterized by the ratio $\lambda = \theta_{\text{Max}}/\theta_0$ of the local angular width of the sides of the finger to the angular width of the cell. At low velocities (Fig. 3) the extrapolation of the finger sides does not cross exactly at the apex of the cell, but behind it (in both the divergent and convergent case). This shows that the maximum width of the finger is a slowly varying function of the distance to the apex and the general finger shape does not have exact self-similarity. At larger velocities the situation becomes simpler. Figures 4(a) and 4(b) show, respectively, in the divergent case with $\theta_0 = 23°$ and in the convergent case with $\theta_0 = -32°$, superimposed photographs of fast fingers. In the region shown by these photographs, the value of λ has remained constant at λ_0 (to the accuracy of the experiment) so that the extrapolations of the linear finger sides now cross at the apex of the cell. Varying the photographic enlargement, we can superimpose exactly successive states of the same finger; the shape of the tip is identical, showing that in this range of velocities the fingers have a self-similar growth.

This is an indication that, in the absence of surface tension, there is an underlying family of exact solutions that has self-similar growth, and that a selection of the type observed in parallel cells takes place. The experimentally observed profiles have well defined shapes that differ somewhat from the solutions of Eq. (8). In the divergent case [Fig. 4(a)] the extremity of the finger given by Eq. (8) is flatter than the observed profile. In the convergent case [Fig. 4(b)] the difference in shape is smaller; the finger given by Eq. (8) has only a slightly sharper tip.

We failed to find an analytical expression for this family of finger shapes in the absence of surface tension. One of us (V.H.) has found such a continuous family of solutions in the particular case where $\theta_0 = 90°$ (his calculation is presented in the Appendix), but comparison with the experiment is not possible; at this value of the angle, as we will show, the growing finger is not stable.

b. Fingers selection. Even though the analytical expression of the fingers' shape is not known, it appears that the selective process that takes place is in continuity with the linear case and can be investigated. In order to do so, we must remember that the parameter $1/B$ changes as the finger moves.

Most of our experiments were performed with a constant applied pressure. For distances r_0 in the range 5–50 cm and in our particular experimental setup, the velocity of the fingers was found to vary as $r_0^{-0.4\pm0.1}$ in the divergent case, and as $r_0^{-1.6\pm0.1}$ in the convergent one. So the decrease of the velocity in the divergent case does not compensate the increase of the width of the cell, and $1/B$ increases constantly as the finger moves out. In the convergent case, on the contrary, $1/B$ decreases slightly during the finger motion.

We have to choose a measurement procedure adapted to this unsteady situation. To investigate the finger selection we will assume that, in the range of low values of $1/B$, we can still measure a *local* finger width as a function of the *local* value of $1/B$. On a given image, when the fingertip has reached a distance r_0 from the origin, the front part of the finger extends over a length of the order of the local width of the cell $W(r_0) = \theta_0 r_0$, so the finger has approximately reached its maximum width at $r_1 = r_0 - W(r_0)$ for divergent fingers and $r_1 = r_0 + W(r_0)$ for convergent ones. We choose to measure the angular ratio λ at this distance r_1 from the origin. In order to show the similarity in behavior with the fingers in a linear cell, we will plot the observed values of $\lambda(r_1)$ as a function of a local value of $1/B(r_1)$,

$$\frac{1}{B} = \frac{12\mu V}{T}\left(\frac{\theta_0 r_1}{b}\right)^2, \tag{11}$$

where $\theta_0 r_1$ is the local width W_1 of the channel and V is the local mean velocity between r_1 and r_0.

Figure 5 shows a cumulative plot of all the measured values of λ in a divergent cell with $\theta_0 = 23°$ for several values of the velocities and at three different positions in the cell. Though there is a certain scatter of the values, the general evolution of λ is similar to the evolution in a linear cell, except for the saturation value λ_0. This supports the procedure we have followed and shows that $1/B$ is the correct parameter for the evolution of λ. The fingers observed at low velocity, which have a spatial variation of λ (Fig. 3), correspond to the range of values of $1/B$ where λ changes rapidly. The self-similar fingers shown on Fig. 4 are observed at values of $1/B$ where λ has practically reached its limit.

The scatter in the results is not a surprise. It is due to a slight dependence of the observed value of $\lambda_0(r_1)$ on the local aspect ratio of the cell $\theta_0 r_1/b$ (which in Fig. 5 ranges 30–120). This is identical to the effect observed by Tabeling *et al.*[23] in linear cells. They found that the values of λ are shifted down by about 5% when the aspect ratio of their cell is changed from $W/b = 112.5$ to $W/b = 34$. We find an effect of the same sign and of the same order of magnitude. They have shown that this shift is due to the perturbing effect of the oil films left on the glass plates. Reinelt[25] and Sarkar and Jasnow[26] have calculated this correction and found quantitative agreement with the experiment. This effect also affects our results, and a numerical simulation or analytical

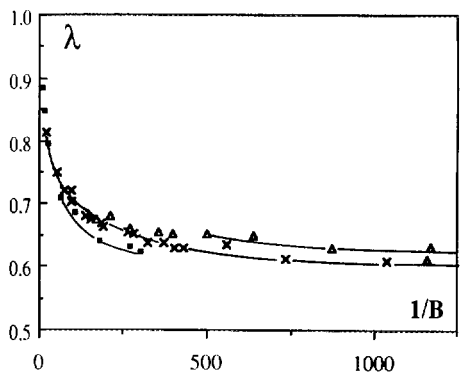

FIG. 5. The evolution of the observed local value of λ, as a function of the local value of $1/B$ in a divergent cell with $\theta_0 = 23°$, in regions of different widths and at various velocities. (■) $W_1 = 30$ mm, $r_1 = 75$ mm; (×) $W_1 = 50$ mm, $r_1 = 123$ mm; (△) $W_1 = 120$ mm, $r_1 = 295$ mm.

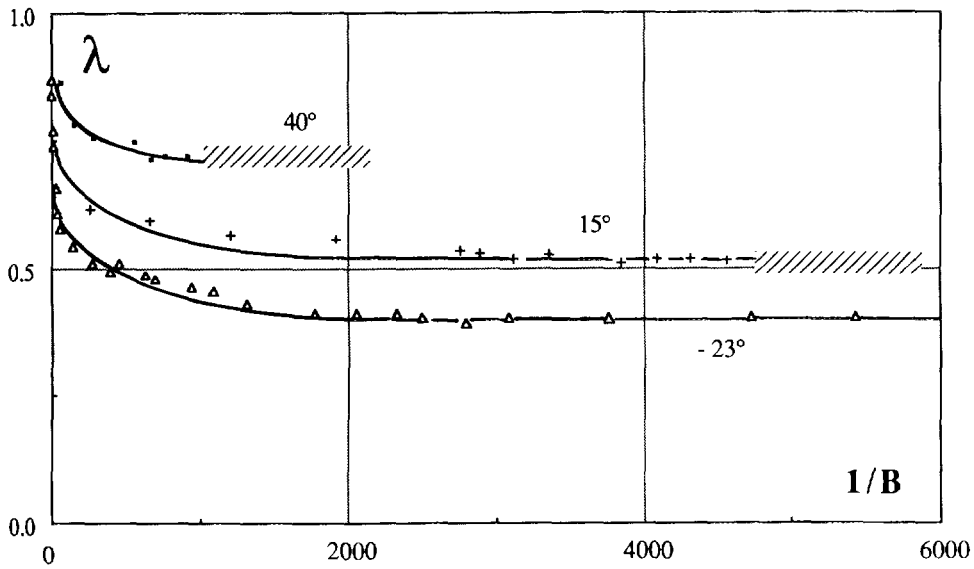

FIG. 6. Experimental evolution of λ with $1/B$. Value taken for the same width $W \approx 12$ cm and for a different angle [(■) $\theta_0 = 40°$; (+) $\theta_0 = 15°$; (△) $\theta_0 = -23°$]. Negative values of θ_0 correspond to convergent cells. The hatched zones correspond to the onset of instability in the first two cases (for the convergent finger this onset is observed at $1/B \approx 15\,000$).

calculus in sector shaped cells would give slightly larger values of λ_0.

The general trend of the evolution of λ is the same for a parallel cell and for a cell with a small angle or a large angle. The stability range and the limit value λ_0 both depend on the angle of the cell, and on whether the finger moves in the divergent or convergent direction. We now wish to study these limit values as a function of the angle. In order to have comparable experimental conditions and to avoid the scatter as a result of different aspect ratio, we will now always consider the region of the cells where the width is about 12 cm and vary the velocity to reach at this point different values of $1/B$.

Figure 6 shows a comparison of the evolution of λ as a function of $1/B$ for two divergent cells of angle 40° and 15°, and a convergent cell of angle $-23°$. In the three cases the evolution for small values of $1/B$ is similar, but the limit values at which the fingers become unstable are very different. This stability limit will be discussed more completely in the next section. It is sufficient here to note that fingers in convergent cells are more stable than in parallel ones, and that divergent fingers become increasingly unstable when the angle of the cell increases. The asymptote where λ saturates at λ_0 is clearly observed for all convergent fingers and for divergent fingers up to a value of the angle of approximately 20°. For larger angles the fingers become unstable before they have reached their limit width. As a result, for divergent fingers the range of near self-similarity reduces and finally vanishes.

Table I gives the smallest values λ_m of λ observed for

TABLE I. Experimental values of minimum width λ_m of instability threshold ($1/B$), and of maximum value of l/l_c, for various values of the cells' angle (negative values of the angle correspond to convergent cells, positive ones to divergent cells).

Angle of the cells (in degrees)	λ_m	Limiting value of $1/B$	l/l_c	First mode unstable
− 90°	0.21 ± 0.01	50 000 ± 10 000	4.3 ± 0.9	side branching
− 60°	0.29 ± 0.01	...	...	side branching
− 32°	0.38 ± 0.01	...	...	side branching
− 22°	0.41 ± 0.01	...	...	side branching
− 15°	0.43 ± 0.01	10 000 ± 2000	3.7 ± 0.8	side branching
− 6°	0.46 ± 0.01	8500 ± 1000	3.9 ± 0.5	side branching
0	0.48 ± 0.01	7000 ± 1000	3.7 ± 0.5	side branching
6°	0.50 ± 0.01	6000 ± 1000	3.6 ± 0.6	side branching
15°	0.53 ± 0.01	5000 ± 500	3.6 ± 0.4	side branching
22°	0.61 ± 0.01	2500 ± 500	2.9 ± 0.6	side branching
23°	0.64 ± 0.01	...	...	side branching
32°	0.70 ± 0.01	1000 ± 100	2.0 ± 0.2	side branching
40°	0.73 ± 0.01	...	...	side branching
44°	0.76 ± 0.01	...	...	side branching
50°	0.75 ± 0.01	...	...	...
56°	0.76 ± 0.01	700 ± 100	1.9 ± 0.3	...
69°	0.85 ± 0.01	...	...	tip splitting
88°	0.85 ± 0.01	100 ± 50	0.8 ± 0.4	tip splitting
105°	0.91 ± 0.01	...	...	tip splitting

stable fingers in all the cells that we used. These values are plotted as a function of θ_0 in Fig. 7 (where negative angles represent the convergent cells and positive ones represent divergent cells). For all the observed convergent fingers $-90° < \theta_0 < 0°$ and for the divergent fingers in cells with $\theta_0 < 20°$ where the measured λ_m coincide with the asymptotic limit λ_0, we find a linear variation that can be written

$$\lambda_0 = 0.48 + (3.25 \pm 0.10)10^{-3}\theta_0 , \qquad (12)$$

where θ_0 is expressed in degrees.

The curve interpolates at $\theta_0 = 0$ at the value $\lambda_0 = 0.48$, which is the limit value observed experimentally in a linear cell of the same width.

For divergent fingers in cells of larger angle $\theta_0 > 20°$, the limit value departs from this linear dependence because the asymptotic value λ_0 cannot be reached before instability. For angles $20° < \theta_0 < 50°$, however, there is still a range where λ varies slowly with $1/B$, so that a near self-similarity is observed. We noticed that at the minimum value λ_m, the width of the oil remaining on the side of various cells was approximately the same:

$$(1 - \lambda_m)\theta_0 /2 \approx 5° . \qquad (13)$$

Indeed the limit value λ_m shown in Fig. 7 for angle $\theta_0 > 20°$ are well fitted by

$$\lambda_m \approx 1 - 10°/\theta_0 .$$

This empirical law is unexplained and could be due to a mere coincidence. However, it will be useful in Sec. IV A. For $50° < \theta_0 < 100°$ it is possible to obtain wide, single divergent fingers, but they are always of the type shown in Fig. 3; their width decreases as they move until they undergo tip splitting.

Altogether, the results presented above show that the selection of the asymptotic solution in sector shaped cells is in continuity with the usual selection in linear cells. The curvature introduced by the geometry affects the whole profile and shifts the selected λ_0. Equation (10) gives the curvature at the tip of the approximate solution (8). A simple conservation of the curvature at the tip would only give a weak dependence of λ_0 on θ_0, and does not account for the selection given by relation (12). A complete calculation of the selective effect of surface tension in these cases will be needed to interpret the results.

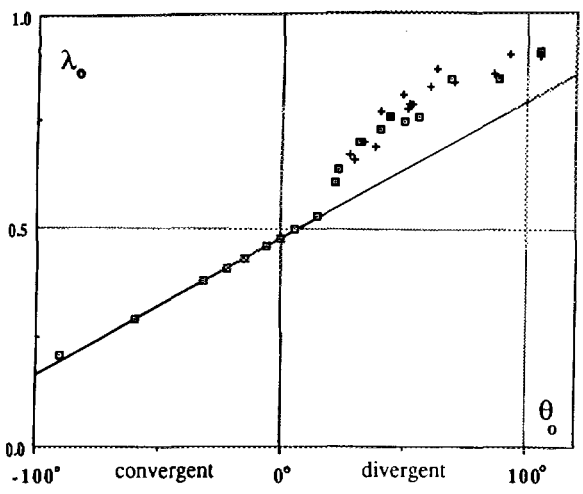

FIG. 7. Evolution of the minimum value λ_m for divergent (positive angles) and convergent (negative angles) fingers as a function of the angle of the cell. (□) results obtained in sector shaped cells; (+) values from radial fingers of primary and secondary patterns obtained in the circular geometry; (—) fit of the asymptotic values λ_0 by relation (12).

3. Fingers stability

Three phenomena are to be considered for the stability of Saffman–Taylor fingers. These are side branching, tip splitting, and screening off. We will first describe the observed thresholds for the first two instabilities in sector shaped cells.

In the discussion of the fingers stability, we will have to compare the actual width of the finger l ($l = \lambda_m W$) to the length l_c:

$$\frac{l}{l_c} = \lambda_m \frac{W}{l_c} = \frac{\lambda_m}{\pi\sqrt{12}} \sqrt{\frac{1}{B}} . \qquad (14)$$

Side branching results from the progressive amplification of a disturbance as it is advected along the curved profile of the finger sides. It is a convective instability with a spatial amplification rate. It is best observed in structures that have a stabilized tip, such as anomalous fingers (Rabaud *et al.*[17]) or crystalline dendrites, where it gives rise to periodic waves. In linear Saffman–Taylor cells, side branching is the first instability to be observed for normal fingers. In this case it only creates, at the threshold, a unique isolated bump. This was observed by Tabeling *et al.*[23] to occur at values of $1/B \approx 7000$ (or $l/l_c \approx 3.7$). It is difficult, however, to establish a threshold for this instability, because it depends on the accuracy with which a distortion of the profile can be detected. Bensimon[27] has shown that the system is exponentially sensitive to the amplitude of the noise incident at the tip, so that the cleanliness of the glass is important in this problem.

The second instability, tip splitting, has such a large growth rate that it divides the fingertip without being advected along the finger side. It was observed by Tabeling *et al.*[23] to occur in linear cells at $1/B \approx 14\,000$. At this value the width of the finger is $l \approx 5.2 l_c$.

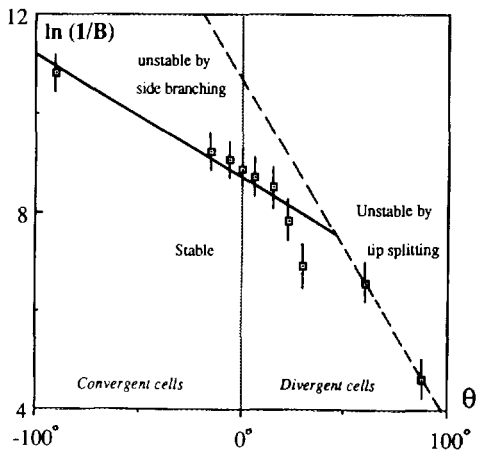

FIG. 8. Logarithmic plot of the instability threshold $1/B$ as a function of the cell's angle: (—) side branching and (- - -) tip splitting.

In sector shaped cells, the measurements of thresholds are more difficult because the value of $1/B$ changes while the finger grows. We choose to measure the local value of $1/B$ where a distortion of the finger became visible. These values of $1/B$ at the threshold are given in Table I and plotted in Fig. 8 as a function of the angle of the cell. In spite of the large uncertainty of the measurements, the general tendencies are clear. In terms of $1/B$, the fingers appear to be much more stable in a convergent cell than divergent ones. This result is partly misleading; it is mainly due to the decreasing values of λ_0 in these cells. If we compare (Table I) the actual width of the finger to the unstable wavelength l_c, we find a much smaller dependence in all the convergent cells and in the divergent ones for $\theta_0 < 20°$. It is only for wider angles that the range of stability of the finger reduces; for values of the order of 80°, the finger becomes unstable as soon as its width becomes of the order of l_c. For wide angles there is also a crossover: whereas side branching was always the first instability to occur, tip splitting becomes dominant in divergent cells with $\theta_0 > 50°$ (Fig. 8).

An explanation can be found in the curvature imposed by the geometry. The configuration of successive isobars in front of growing fingers in a divergent cell and a convergent cell, respectively, are necessarily different. In the divergent case, the fingertip is relatively flat and the pressure gradient in front of the finger is almost the same over a wide zone. Tip splitting, therefore, does not require a strong disturbance of the tip. In contrast, in the convergent case, the curvature of the isobars near the fingertip and near the apex of the cell are of opposite sign and the pressure gradient along the axis of the cell is enforced. It creates a focusing effect and a strong "geometrical anisotropy" that inhibits tip splitting.

In the preceding discussion we have taken the terms side branching and tip splitting in their usual sense. If we analyze very unstable patterns obtained in various geometries we are led to conclude that the distinction between the two processes is not clear cut. The experiments of Park and Homsy[22] and the numerical simulations of Liang[28] have shown that during the nonlinear growth following a tip splitting, there always exists an infinitesimal difference between the two resulting fingers, so that one of them will be screened off and stopped. At this point it appears rather to have been a large side branch of the main finger. In the parallel configuration all the tip splitting finally fails in this way and only one path connects the two ends of the cell. This is not always the case; in the sector shaped cells of a very large angle, the two fingers resulting from a tip splitting finger will both survive. This process will be commonly observed during the pattern's growth in the circular cells.

B. Anomalous fingers

1. Width and shape

We have described in previous articles (Couder *et al.*[16] and Rabaud *et al.*[17]) three different techniques by which the tip of a growing finger can be locally disturbed so that the regime of growth is completely changed. An anomalous finger of this type is selected by its radius of curvature ρ at the tip. In a large range of velocity, ρ is scaled on the capillary length, so that $\rho \propto V^{-1/2}$. (At very large velocities a saturation is observed when ρ becomes of the order of magnitude of the cell's thickness; it then remains constant at $\rho \simeq 2.2b$.)

In the present work we have stretched a thin wire from the origin to the periphery of the cell along its axis to obtain anomalous fingers in sector shaped cells.

Figures 9(a) and 9(b) show a stable and an unstable divergent finger obtained in a cell with $\theta_0 = 30°$. The injection was performed at a regulated pressure and the velocity of the finger was approximately constant in the observed region. As in the linear geometry, the anomalous fingers are narrower than normal ones and more stable. The fingers are not self-similar and they do not show well defined asymptotes. In the divergent case, the relative angular width λ occupied by the finger decreases as it grows; in the convergent case it increases. The fact that they are, more than normal fingers, sensitive to the unsteadiness of the experimental condition, is a result of their specific selection mechanism. In both cases, as the finger velocity is nearly constant, the finger cannot have self-similarity. Instead, the finger width λ increases or decreases continuously so as to maintain a constant curvature at the tip.

This is a direct confirmation of the difference in the selection process of normal and anomalous fingers. Normal fingers are scaled on the cell's width and, in a sector shaped cell, they tend to lead to self-similar solutions even when $1/B$ varies. Anomalous fingers are scaled on the capillary length and would only be self-similar if $1/B$ was kept constant by specific injection conditions. (This could only be realized in the regime where $\rho \propto V^{-1/2}$ if the injection condition gave the finger a velocity $V \propto 1/r_0^2$.)

2. Stability

The parabolic tip of anomalous fingers is very stable as a result of the artificial local anisotropy introduced by the wire. The process of the side branching has been described elsewhere in the case of linear cells (Rabaud *et al.*[17]). It results from the selective amplification of perturbation incident at the tip, amplified in the parabolic region of the finger and damped further. In linear cells, the Saffman–Taylor solutions given by Eq. (1) can be approximated by a parabola near the tip. The extent of the region to which this approximation is valid increases with decreasing λ. Observations in the sector shaped cells are thus well explained: a divergent finger always destabilizes at some point, because λ decreases constantly. In the convergent cells λ increases, the fingers are more and more stabilized by the walls, and side branching becomes inhibited as the finger approaches the center. In both cases the lateral spacing of the side branches is scaled on ρ.

IV. CIRCULAR GEOMETRY: RESULTS AND INTERPRETATION

We have obtained in sector shaped cells (in spite of the lack of exact solutions) clear cut results about the fingers' width selection and about their stability. We will now show in this second part that these results permit an accurate description of the evolution of the patterns in the circular geometry. We must first briefly recall the situation of the problem.

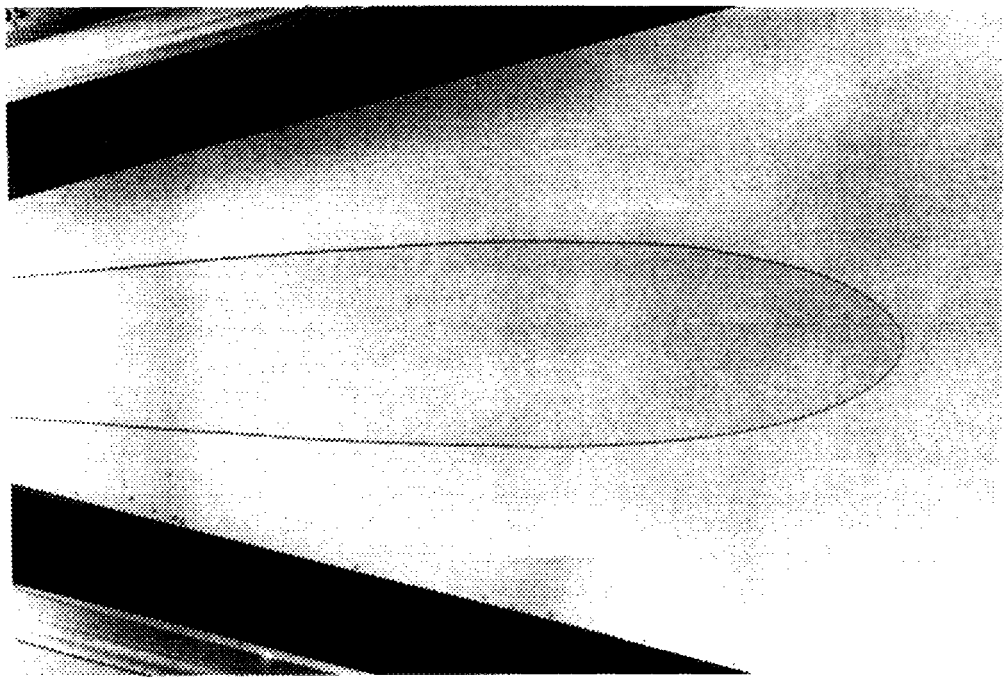

(a)

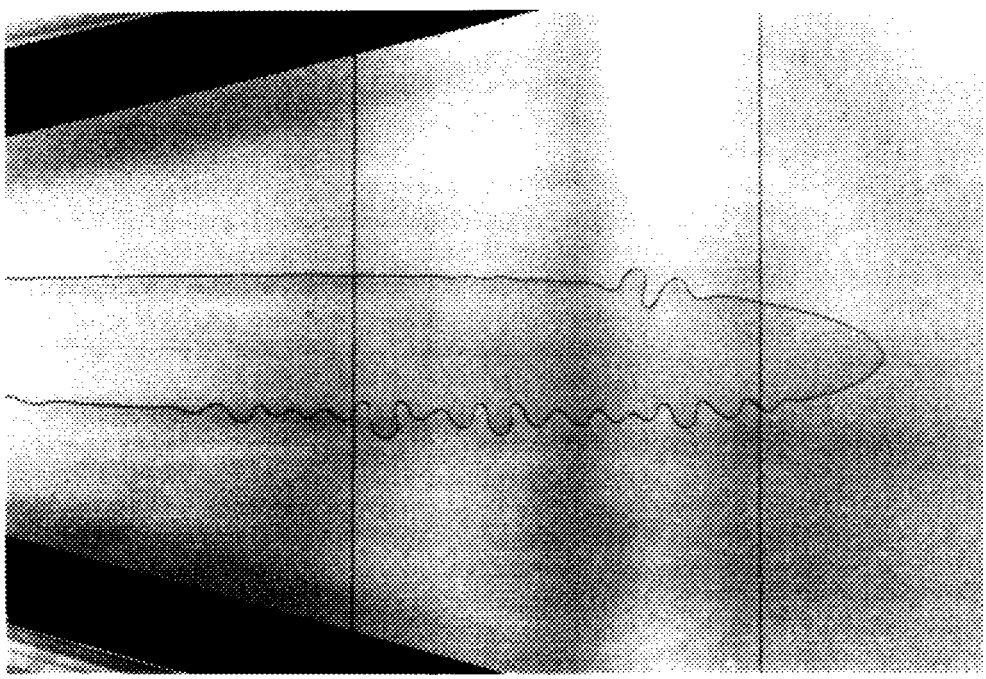

(b)

FIG. 9. Anomalous fingers obtained when a thin wire is stretched along the axis of a divergent cell, $\theta_0 = 30°$; (a) at low velocity and (b) at large velocity.

As noted above the main experimental results in this case are due to Bataille[2] and to Paterson.[3] The theoretical problem has been approached in several ways.

In the first attempt to interpret the finger shapes observed in the circular geometry, Paterson used a conformal transform approach. He suggested that the finger shapes observed in the circular geometry were fitted by solutions that he wrote,

$$(r/r_0)^{\alpha} = \cos p\theta\,,$$

where α and p were fitting parameters.

This solution is identical to our Eq. (8). In our terminology p is $\pi/(\theta_0\lambda)$ and α is $\pi/[\theta_0(1-\lambda)]$. Though this solution fits to a reasonable approximation the finger shapes obtained for small angles θ_0, they are not exact solutions of the problem for the reasons discussed above (Sec. III A 1).

Paterson's presentation, leaving both α and p free fitting parameters, did not give a relation between λ and θ_0. Consequently, a selection of the finger width by the value of the sector angle and the similarity with the parallel cell did not appear.

A completely different approach has also been tried. The search for solutions in the absence of surface tension consists in solving a Stefan problem. A field must be found that satisfies the Laplace equation in a system having boundaries that move with a velocity proportional to the gradient of the field itself.

Shraiman and Bensimon[29] and Sarkar[30] had shown that generally, in the absence of surface tension, the evolution of a front with a polynomial shape "blows up" and leads to the formation of cusplike singularities in a finite time. Howison[4] and Bensimon and Pelcé[5] found, using a complex variable method, that there existed nontrivial solutions that do not blow up in this way. In the axisymmetric case, by introducing m poles in the complex plane, they obtain an m-fold periodic pattern where the interface stops moving in m regions, forming tongues of oil.

Finally, the statistical properties of complex patterns obtained at large velocities have been investigated by Ben Jacob *et al.*,[7] Sander,[8] and Rauseo *et al.*[9] in relation to the current interest in fractal structures. The results that we present here cannot be compared to theirs, as we limit ourselves to initial stages of the growth, where no scale of the pattern ever becomes very large compared to the capillary scale.

A. Divergent flow

1. Velocity profile

Before investigating its destabilization, we first sought the velocity of a stable circular front. Here we consider the case where the cell is initially full of oil and where the injection is through a pinhole at the center of the cell. In the case of a constant volumic rate of injection Q, mass conservation gives the velocity V of an interface of radius r,

$$V = (Q/2\pi b)(1/r) . \tag{15}$$

With this type of injection, the velocity is infinite at the initial time and decreases steadily through the cell.

Experimentally, it is easier to have a pressure controlled injection. In this case, if P_1 is the injection pressure of air and P_2 the oil pressure at the external boundary of the cell of radius R, it is easy to solve the Laplace equation for the isobars, and Eq. (2) gives the velocity at the interface,

$$v(r) = b^2(P_1' - P_2)/12\mu r \ln(R/r) , \tag{16}$$

where $P_1' = P_1 - T(2/b + 1/r)$ takes into account the surface tension induced pressure drop ($2/b$ is the vertical curvature of the interface and $1/r$ the horizontal one). As we inject with a hole of diameter larger than b,

$$P_1' \approx P_1 - 2T/b .$$

Equation (16) shows that the velocity, initially very large, decreases rapidly and remains almost constant (within 10%) for $0.2 < r/R < 0.6$ and diverges near the outer border when r tends to R.

Equation (16) can be integrated (for $r \gg b$) and we obtain the following relation $r(t)$:

$$\left(\frac{r}{R}\right)^2\left[2 - \ln\left(\frac{r}{R}\right)\right] = \left(\frac{b}{R}\right)^2 \frac{P_1' - P_2}{\mu} t . \tag{17}$$

2. First and second destabilization

During the growth, the stability of the circular front is related to the ratio of its perimeter $L(t) = 2\pi r(t)$ to the capillary length scale l_c given by relation (6). With the assumption that the linear analysis of Chuoke *et al.*[26] is still valid for a curved interface, the front is certainly stable whenever this ratio is smaller than unity.

With a constant volumic rate of injection, using relation (15) we find

$$L/l_c = \sqrt{(2\mu Q/\pi T b^3)}\,\sqrt{r} . \tag{18}$$

With a constant injection pressure, using relation (16) we find

$$\frac{L}{l_c} = \sqrt{\frac{P_1' - P_2}{3T}}\sqrt{\frac{r}{\ln(R/r)}} . \tag{19}$$

The two possible evolutions of L/l_c are shown in Fig. 10 for typical arbitrary values of the experimental parameters. In both cases the ratio grows with $r(t)$. In an ideal radial motion the front is stable near the center where $L/l_c < 1$ and becomes unstable as it moves out. At large injection rates it is difficult to maintain this initial stable state, because the radius of the injection hole is no longer negligible compared to l_c. This nonideal situation can also be obtained purposefully when a circular bubble is present at the center before the beginning of the injection. Unless specifically stated, all the following description refers to the situation of an ideal radial motion with negligible size of the injection hole.

The initial destabilization can be observed easily at low injection rate. Usually the first noticeable deviation from circularity corresponds to an n-fold symmetry with $n = 3$. However, this initial deformation does not lead to the forma-

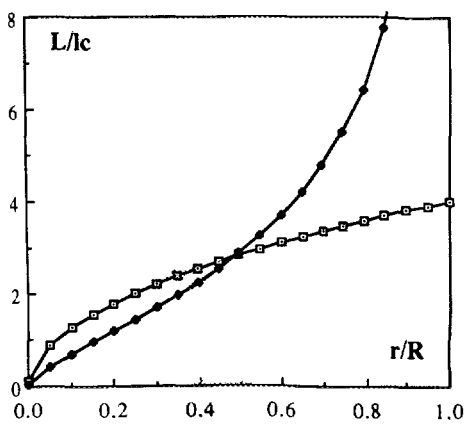

FIG. 10. The evolution of the ratio of the perimeter of the circular front L over the capillary length scale l_c, as the front moves outward in a cell of radius R. (□) injection at constant volumic rate [Eq. (18)]; (◆) injection at constant pressure [Eq. (19)].

tion of a corresponding number of fingers. As the front keeps moving outward, other modes with larger values $n = 4$ and 5 become unstable and grow. Figure 11 shows the front at this stage. It is irregular for two different reasons; its deformation results from the superposition of the first three modes, and it is related to the imperfection of the cell. No matter how carefully the cell has been built, there are always small imperfections in the state of its surfaces that are determinant in the excitation of the instability. This can be induced from experiments where all the injection conditions are exactly reproduced. The patterns obtained in two different runs, though irregular, are very similar to each other.

The separation in fingers occurs when the dips formed in the slow parts of the front become deep enough so that screening off is dominant. These regions of the front are no longer submitted to a dynamical pressure gradient and they become practically motionless. At this point the waves have entered the nonlinear regime of growth, which gives rise to a pattern of fingers.

The circular front is, from then on, divided into several independent sections by these motionless regions, often called fjords, in which the oil remains blocked. In the ideal case, the initial number n_1 of fingers ranges between five and seven. (A larger number of fingers is observed if a finite circular motionless front exists in the cell when the fluid motion starts.) Figure 12 shows one of these patterns at three stages of its growth. Several important characteristics can be noted.

The primary fingers do not tend to screen each other off and they have the same velocity so their outer envelope remains circular. As they grow, their width increases so that they become unstable. When their width becomes of the order of $2l_c$, tip splitting occurs. If all the n_1 sectors were equal, all the tip splitting would be simultaneous and the pattern would be very regular; but the initial pattern is somewhat irregular and the broader the finger the more unstable it is. On the whole, the formation of these secondary fingers results in a larger pattern with $n_2 \simeq 2n_1$. Here we limit ourselves to these primary and secondary patterns.

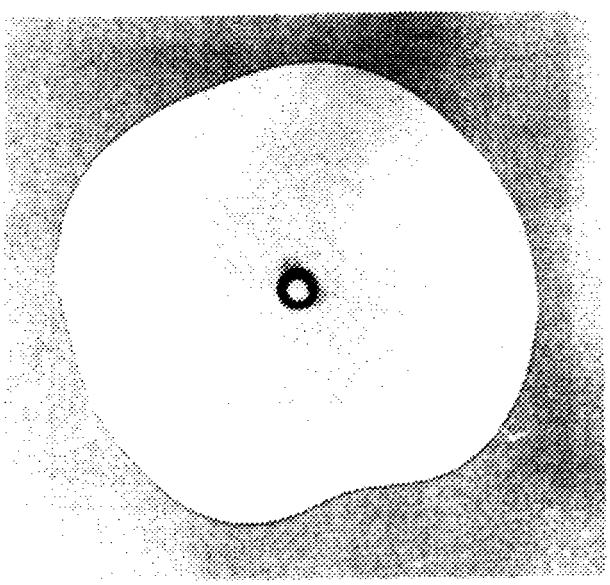

FIG. 11. The initial destabilization of the circular front.

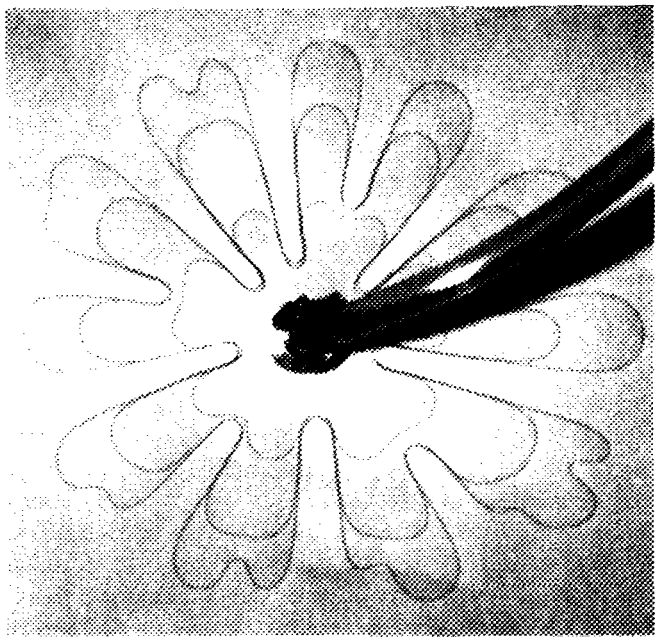

FIG. 12. Photograph of three successive states of a pattern obtained for a divergent flow in a circular cell.

If we examine the shape of one of the fingers (Fig. 13), three regions can be distinguished in its interface. Region I corresponds to the blocked zone where the screening off is total. There is a very slow change in the shape of this zone under the smoothing influence of surface tension. It takes the shape of an arc of a circle with a radius that increases slowly with time. Region II corresponds to the sides of the finger, and region III to its tip.

An important element for the interpretation of the shape of these fingers is that their lateral sides are straight lines that can be extrapolated and usually cross at the center of the cell. In order to show how the results of Sec. III can be used to interpret the shape of these fingers we have to recall the discussion by Saffman and Taylor[1] of their experiment. They grew a single finger in a linear channel. Seeking analytical solutions of the interface, they replaced the actual lateral boundaries by a periodic condition so that they considered an infinite set of equal fingers growing in parallel cells at the same speed. They argued that on the straight line halfway between neighbors there is no transverse component of the velocity, so that the effect of the lateral walls is reproduced. This possibility of replacing the lateral walls by a periodic boundary condition has since been used in many numerical simulations of Hele–Shaw flows.[21]

We use the same argument in reverse. When the neighboring radially growing fingers are of similar width and advance at the same speed, we do have periodicity in the orthoradial direction. We can thus draw (Fig. 13) radial lines along the bisectors of the angle formed by the sides of the neighboring fingers. Because of the symmetry, there is no motion of oil across these lines and they could, without

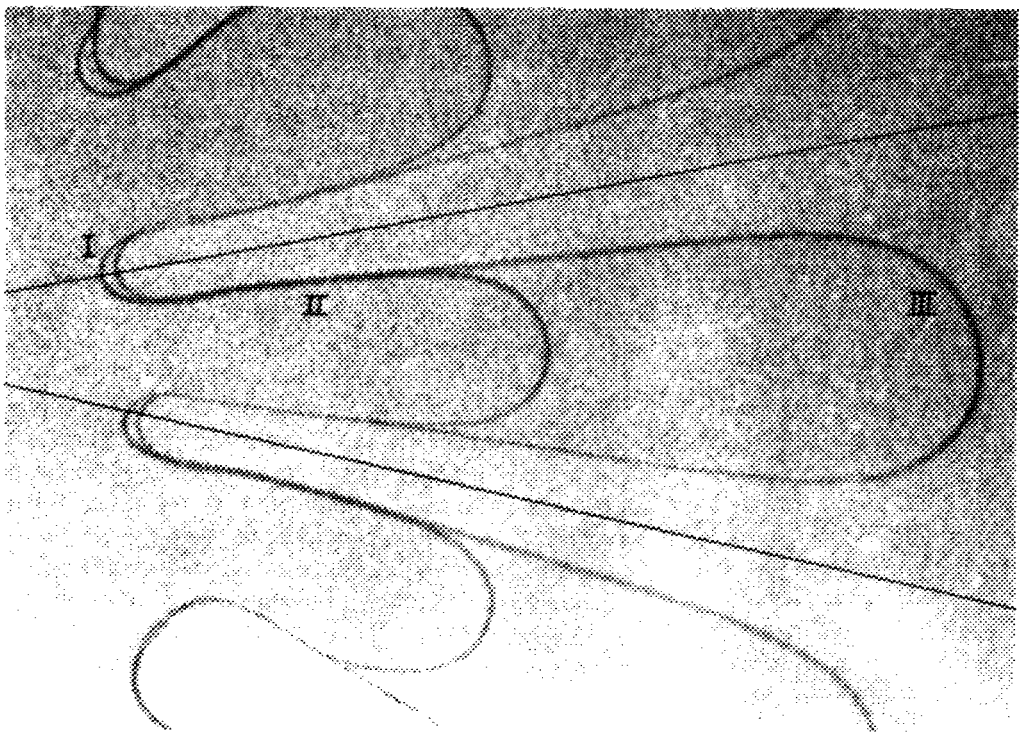

FIG. 13. Detail of a finger obtained in a circular cell showing the three regions of its front and the virtual sector shaped cell (—) in which it grows. This virtual cell has an angle of $\theta_0 = 23°$ and the finger shape is identical to that obtained in a sector shaped cell of the same angle shown in Fig. 4(a).

changing the flow, be replaced by walls. We can therefore consider that the growth of the primary fingers occurs in n_1 sector shaped cells limited by virtual radial walls.

The fingers resulting from the tip splitting can, in turn, be considered as growing in sector shaped cells of smaller angle. It is worth noting that, as shown in Fig. 12, the two lateral sides of the initial finger are apparently not affected by its division. The two outer sides of the secondary fingers are aligned with those of the primary one.

We can now compare each finger's shape, width, and stability with those observed in sector shaped cells of the same angle. Figure 13 was chosen because the angle of the virtual cell $\theta_0 = 23°$ is the same as the angle of the real cell shown in Fig. 4(a). The profiles of the fingers obtained in both cases can be superposed, showing their strict identity. The only difference is that in the circular geometry there exists the blocking zone I. This suppresses the region, observed near the apex of sector shaped cells, where $1/B$ is small and where λ has not reached its limit value. The fingers' sides are linear and extrapolate at the center as only the region where their width has reached its asymptotic value is observed.

In each of these virtual sector shaped cells, we measured the ratio of the angular width of the air finger to θ_0. The observed values, plotted in Fig. 7 as a function of θ_0, are the same as the limit values λ_m that we observed in real sector shaped cells.

Finally the limit values of $1/B$ at which a finger becomes unstable and its instability type (tip splitting or side branching) are also in agreement with those observed above.

The previous argument is only strictly valid when the neighboring fingers have similar angular widths. If such is not the case, the symmetry argument is no longer valid and, *a priori*, there would be no reason for the bisector of the fjord to be a virtual wall. Let us consider two fingers next to each other and the fjord in between them. Our experimental results lead us to conjecture that there is still a virtual wall and that the width of these fingers can be written, respectively, $\lambda^1_m\theta_1$ and $\lambda^2_m\theta_2$. The wall then has to divide the angle of the fjord in the ratio $(1-\lambda^1_m)\theta_1/(1-\lambda^2_m)\theta_2$. The procedure to determine θ_1 and θ_2 and to fix the virtual walls turns out to be very simple because of the empirical law (14): in practice $(1-\lambda^1_m)\theta_1 \approx (1-\lambda^2_m)\theta_2$, so that the virtual walls can still be chosen along the bisector of the fjords. The analysis of various patterns confirms the validity of this procedure.

The present results differ markedly from the characteristics of the model proposed by Howison[4] and Bensimon and Pelcé[5] where the fjords have parallel sides. This would only be obtained in our description for $\lambda = 1$, a limit where the angular width of the fjord would be zero. The finite constant thickness of the fjord in their model is due to the introduction of a fitting parameter, whereas the experimental evidence points toward a radial structure of the fjords with $\lambda < 1$.

The results that we obtained about the finger selection can be used to predict some general characteristics of the circular patterns. When the pattern grows, the number of virtual cells increases, the limit values of λ become smaller,

and the finger will have a larger stability. (Figure 12 shows that secondary fingers are observed longer.) From the change in the selected values of λ in each cell results a change in the statistical properties of the pattern. When we draw a circle centered at the origin, it cuts the fingers and we can measure the proportion p_a of its perimeter occupied by air fingers,

$$p_a = \langle \lambda \rangle = \frac{\Sigma_{i=1}^{n_f} \lambda_i \theta_i}{2\pi}, \tag{20}$$

where the summation is extended to the n_f fingers.

From the dependence $\lambda_m(\theta_0)$ (Table I) we can deduce, for ideal patterns formed of n_f equal cells, the expected dependence $p_a(n_f)$. The values measured on actual patterns after their first and second destabilizations have been plotted in Fig. 14 as a function of the number of fingers. The cells' angles are not really equal, but the observed values p_a are in good agreement with those predicted. For primary patterns p_a is of the order of 0.8, for secondary ones $p_a \approx 0.6$.

This result shows how the effect of surface tension affects the overall aspect of the pattern. Because the selective action of surface tension is related to the curvature, the statistical properties of a region of an axisymmetric pattern, in the initial stages of its growth, will depend upon the distance of this region to the center.

3. Further evolution

The secondary fingers correspond to virtual sectors of angular width of the order of 20°–30°. For these values of the angle we have seen, in Sec. III A 3, that the first instability to appear is side branching. This is also observed here. The side branches have a direction of growth that forms an angle with the radial direction; they can now reach large amplitudes but they usually do not lead to the formation of long-lived fingers. The main directions of growth are radial, and the original primary and secondary cells continue to divide the pattern far from the center and define the main directions of growth. Each of these cells is filled with a very unstable chaotic finger that generates constantly new side branches. The study of the resulting large scale patterns is beyond the scope of the present paper and will be developed elsewhere.

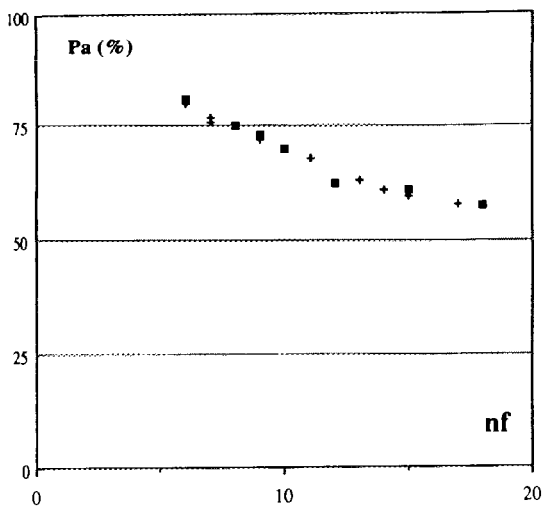

FIG. 14. The occupation of the cell by air as a function of the number of fingers. The points (■) are deduced from the values of λ_m shown in Fig. 7 with the hypothesis of patterns formed of equal fingers. The experimental points (+) correspond to values measured in real patterns.

B. Convergent flow

In order to avoid disturbance by the spacers, the experimental procedure had to be adapted. During the first filling of the cell we inject oil at the center and stop the injection when it has invaded a circular region of radius $R_1 < R$. Then we siphon the oil out of the center. The circular front destabilizes at a wavelength scaled on l_c. As the perimeter of the circle reached by the fingertips shrinks, the fingers tend to be pushed against each other and the further evolution is characterized by systematic competition between the initial fingers. In the moderate range of velocity we investigate here, no tip splitting or side branching occurs. (Side branching is observed to occur at very large velocity, but always gives rise to very short-lived branches.) There is a hierarchy of successive screening off, shown on Fig. 15, and only one finger will reach the center. Even though the last finger moves in a wide cell with $\theta_0 = 360°$, the finger does not widen. (As mentioned before there is a strong focusing effect; the isobars curvatures, near the fingertip and near the apex of the cell, are of opposite sign so that the pressure gradient along the axis of the finger is enhanced.) The experiments performed in sector shaped cells are not very useful here in interpreting the shapes and width of the fingers. The virtual cells cannot be defined, because the strong competition between neighbors constantly break the orthoradial symmetries. The fingers are always in transient states because their environment changes constantly.

V. CONCLUSION

In the present article we have shown that, in sector shaped cells, the width of Saffman–Taylor fingers is selected by a process that appears in continuity with the selection classically observed in the parallel cells. Though we could not find them, except in the particular case where $\theta_0 = 90°$, it is likely that there is an underlying family of self-similar solutions. Even when it is small, the effect of surface tension is to select among these a particular solution. In comparison with the parallel case, a divergent finger profile of a given λ tends to be more bent by the geometry. This could explain that in reaction, fingers with larger relative width λ_0 are selected. A finger moving in the convergent direction is submitted to less curvature constraint from the boundaries, so that narrower solutions can exist.

The stability of the fingers is also affected by the geometry. For divergent fingers the instability threshold is lowered and tip splitting becomes the dominant instability because the fingertip becomes broader. Convergent fingers are more stable than parallel ones and tip splitting is practically inhibited.

We have also shown that these results permit an accurate description of the simple divergent patterns obtained in circular cells. After the first destabilization of the front, a

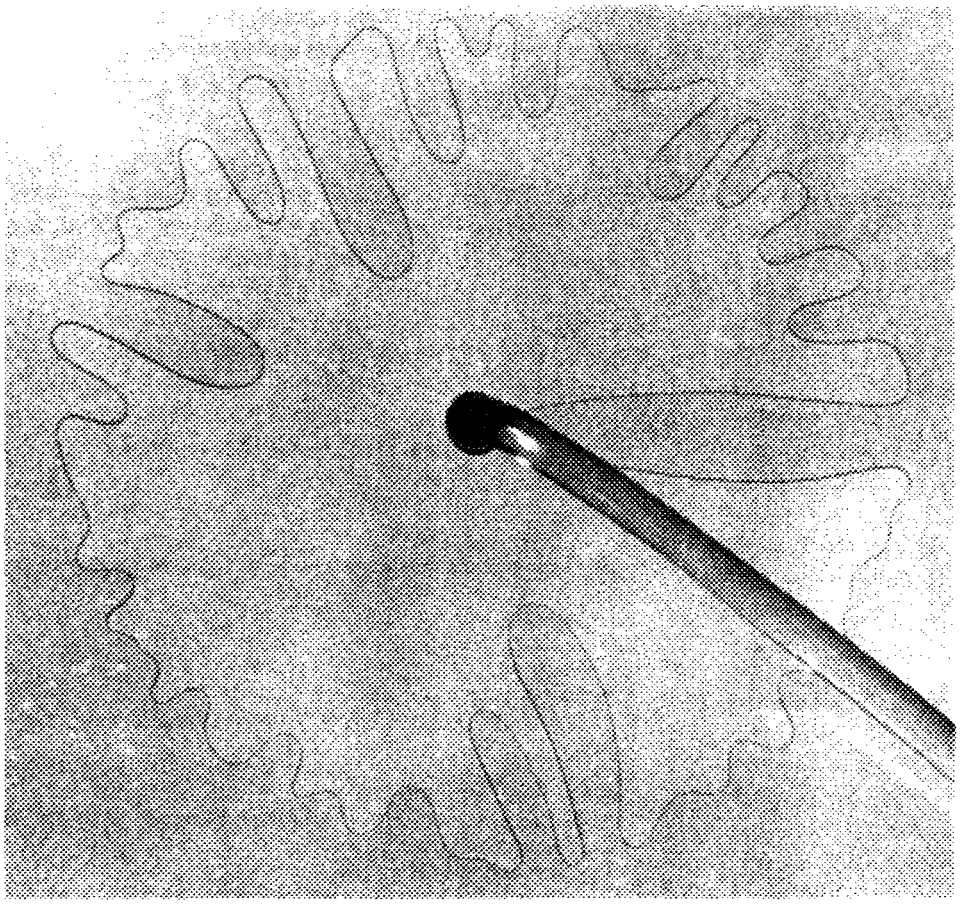

FIG. 15. Photograph of a typical pattern obtained for a convergent flow in a circular cell. The photograph was taken when the fastest finger has reached the center. All the other fingers have been screened off and are motionless.

number n_f of fingers are formed and the further evolution occurs as if the disk was divided in n_f cells. In each of these virtual cells the finger shape and selection correspond to what is observed in real sector shaped cells of the same angle. The rate of occupancy of the circular cell by air, and its evolution during the growth of the pattern, can be deduced from the fingers selection.

ACKNOWLEDGMENTS

Several questions investigated in the present work arose during two projects realized with O. Cardoso, D. Dupuy, P. Tavernier, W. Thom, and V. Marecal, students at University Paris 7. We also thank C. Caroli, N. Gerard, and A. Pumir for helpful discussions during this work.

APPENDIX: EXISTENCE OF THE MATHEMATICAL SAFFMAN–TAYLOR FINGERS IN NONPARALLEL GEOMETRY

The experiment described in the main text led us to wonder whether the results that have been obtained[1,13–15] for a finger moving in a parallel channel could be generalized to nonparallel geometries. A first step in this direction would be to find the equivalent of the Saffman–Taylor continuum family. This is, however, more subtle than appears at first sight, as we explain later, and our findings have been very partial.

As is well known (see Ref. 10 for a review), the motion of the interface satisfies

$$v_n = \mathbf{n}\cdot\nabla\phi\,, \tag{A1}$$

where ϕ is the velocity potential such that

$$\nabla^2\phi = 0\,. \tag{A2}$$

The boundary conditions on the velocity potential are

$$\phi = +\gamma\kappa \tag{A3}$$

on the finger interface (κ is the local curvature of the one-dimensional interface and γ a parameter proportional to the surface tension) and $\nabla\phi$ is parallel to the side of the channel (so that no fluid escapes from the cell).

We are interested in obtaining an exact self-similar solution of the above equations. Let us first consider the zero-surface-tension case (i.e., $\gamma = 0$) with a constant extraction rate at infinity normalized to 2π by convention, i.e.,

$$\phi \sim (2\pi/\theta_0)\log\sqrt{x^2+y^2}\,, \quad \text{when } x^2+y^2 \to \infty\,.$$

It is convenient[1,10] to use the hodograph method and consider $z = x + iy$ as an analytic function of the complex velocity potential $\omega = \phi + i\psi$. The interface equation of motion (A1) is just

$$\left(\frac{\partial x}{\partial t}\frac{\partial y}{\partial \psi} - \frac{\partial y}{\partial t}\frac{\partial x}{\partial \psi}\right) = 1, \quad \text{on } \phi = 0\,. \tag{A4}$$

For an exactly self-similar motion $x(t,\phi=0,\psi) = f(t)x(\phi)$, $y(t,\phi=0,\psi) = f(t)y(\psi)$, this reduces to (with a suitable choice of the time zero)

$$\mathrm{Im}\left(z^*\frac{\partial z}{\partial \psi}\right) = 1 \tag{A5}$$

(where z^* is the complex conjugate of z), while f satisfies

$$f(t)\frac{df(t)}{dt}=1, \quad \text{i.e., } f(t)=\sqrt{2t+1}\,.$$

The normalization has been chosen such that the side of the channel is located at $\psi=\pm\pi$. The mathematical problem of finding the self-similar equivalent of the well-known constant velocity Saffman–Taylor solution in a parallel channel has thus been reduced to finding an analytic function z in the semi-infinite strip $\phi\geqslant 0$, $-\pi<\psi<\pi$, such that (i) $\arg z=\pm\theta_0$ on the half-lines $\psi=\pm\pi$ (the side boundary of the cell), (ii) $z\sim\exp(\omega\theta_0/2\pi)$ when $\phi\to+\infty$, and (iii) z satisfies Eq. (A5) on the segment $\phi=0$.

The whole difficulty and difference with the usual case is that (A5) is a nonlinear condition. This is a kind of nonlinear Riemann–Hilbert problem, and we do not know of any general method to handle it.

The approximate finger shape obtained by conformal transformation [Eq. (8) of the main text] reads in our notation

$$z=\xi^{\theta_0/2\pi}(1+\xi^{-1})^{(\theta_0/\pi)(1-\lambda)}, \quad \text{with } \xi=\exp\omega\,.$$

This satisfies conditions (i) and (ii) but does not satisfy (iii), contrary to what is asserted in Ref. 3. [The problem is that v_n transforms like a length under the conformal transformation, but $\nabla\phi$ transforms like the inverse of a length so (A1) is no longer satisfied after a conformal transformation if the local dilatation factor is not constant.] It is possible to correct this defect for $\theta_0=\pi/2$. In this particular case it is easy to check that a continuous family of solutions is given by

$$z=\xi^{1/4}[(1-\xi^{-1/2})^{(1-\lambda)/2}(1+\xi^{-1/2})^{(1+\lambda)/2} + (1-\xi^{-1/2})^{(1+\lambda)/2}(1+\xi^{-1/2})^{(1-\lambda)/2}]\,,$$

for $0\leqslant\lambda\leqslant 1$. This suggests that the analog of the Saffman–Taylor family exists for any angular cell. Unfortunately, we have not yet succeeded in guessing the solutions for values of θ_0 not equal to $\pi/2$.

As a last remark, we note[31] that for nonzero surface tension, arcs of circle are the only exactly self-similar solutions of Eqs. (A1), (A2), and (A3) when a constant extraction rate is imposed at infinity. Indeed in that case, the conservation of mass implies that the dilatation factor f satisfies

$$f\frac{df}{dt}=Cte\,,$$

which in turn implies that $v_n(t)=1/f\,v_n(0)$. This is a Neumann condition for ϕ, on the finger interface. The unique solution of the Laplace equation that satisfies this boundary condition on the interface, together with the other conditions on the side of the channel and at infinity, is

$$\phi(x,y,t)=\phi(x/f(t),y/f(t),0)+a(t)\,,$$

where $a(t)$ is a time-dependent constant.

This is compatible with Eq. (A3) only if $\gamma=0$ or if κ is a constant, that is, for an arc of circle. Therefore a necessary condition for the existence of exactly self-similar solutions at arbitrary γ is to impose a time-dependent extraction rate. In fact, the previous argument read in reverse order shows that the extraction rate should evolve in time as $t^{-1/3}$. This last remark is, of course, not in contradiction with the experimental results. If these self-similar interface solutions tend to an asymptotic shape for a high time-dependent extraction rate, then this shape would also be the one seen with a constant extraction rate.

[1] P. G. Saffman and G. I. Taylor, Proc. R. Soc. London Ser. A **245**, 312 (1958).
[2] J. Bataille, Rev. Inst. Pet. **23**, 1349 (1968).
[3] L. Paterson, J. Fluid Mech. **113**, 513 (1981).
[4] S. D. Howison, J. Fluid Mech. **167**, 439 (1986).
[5] D. Bensimon and P. Pelcé, Phys. Rev. A **33**, 4477 (1986).
[6] S. N. Rauseo, P. D. Barnes, and J. V. Maher, Phys. Rev. A **35**, 1245 (1987).
[7] E. Ben Jacob, G. Deutscher, P. Garik, N. D. Goldenfeld, and Y. Lareah, Phys. Rev. Lett. **57**, 1903 (1986).
[8] L. M. Sander, in *Fractal in Physics*, edited by L. Pietronero and E. Tossatti (North-Holland, Amsterdam, 1986), p. 241.
[9] P. G. Saffman, J. Fluid Mech. **173**, 73 (1986).
[10] D. Bensimon, L. P. Kadanoff, S. Liang, B. I. Shraiman, and C. Tang, Rev. Mod. Phys. **58**, 977 (1986).
[11] G. M. Homsy, Annu. Rev. Fluid Mech. **19**, 271 (1987).
[12] J. M. Vanden-Broeck, Phys. Fluids **26**, 2033 (1983).
[13] R. Combescot, T. Dombre, V. Hakim, Y. Pomeau, and A. Pumir, Phys. Rev. Lett. **56**, 2036 (1986); Phys. Rev. A **37**, 1270 (1988).
[14] B. Shraiman, Phys. Rev. Lett. **56**, 2028 (1986).
[15] D. C. Hong and J. Langer, Phys. Rev. Lett. **56**, 2032 (1986).
[16] Y. Couder, N. Gerard, and M. Rabaud, Phys. Rev. A **34**, 5175 (1987).
[17] M. Rabaud, Y. Couder, and N. Gerard, Phys. Rev. A **37**, 935 (1988).
[18] G. Zocchi, B. E. Shaw, A. Libchaber, and L. P. Kadanoff, Phys. Rev. A **36**, 1894 (1987).
[19] A. R. Kopf-Sill and G. M. Homsy, Phys. Fluids **30**, 2607 (1987).
[20] D. C. Hong and J. Langer, Phys. Rev. A **36**, 2325 (1987).
[21] G. Tryggvason and H. Aref, J. Fluid Mech. **154**, 287 (1983).
[22] C. W. Park and G. M. Homsy, Phys. Fluids **28**, 1583 (1985).
[23] P. Tabeling, G. Zocchi, and A. Libchaber, J. Fluid Mech. **177**, 67 (1987).
[24] R. L. Chuoke, P. Van Meurs, and C. Van der Pol, Trans. AIME **216**, 188 (1959).
[25] D. A. Reinelt, Phys. Fluids **30**, 2617 (1987).
[26] S. K. Sarkar and D. Jasnow, Phys. Rev. A **35**, 4900 (1987).
[27] D. Bensimon, Phys. Rev. **33**, 1302 (1986).
[28] S. Liang, Phys. Rev. A **33**, 2663 (1986).
[29] B. Shraiman and D. Bensimon, Phys. Rev. A **30**, 2840 (1984).
[30] S. K. Sarkar, Phys. Rev. A **31**, 3468 (1984).
[31] The following argument was pointed out by A. Pumir (private communication).